JOURNAL OF Materials CHEMISTRY

Inorganic–organic hybrids by exfoliation of MoS_2 †

Anthony V. Powell,* Laura Kosidowski and Andrew McDowall

Department of Chemistry, Heriot-Watt University, Edinburgh, UK EH14 4AS. E-mail: A.V.Powell@hw.ac.uk; Fax: +44 (0)131 451 3180

Received 18th September 2000, Accepted 7th January 2001
First published as an Advance Article on the web 2nd March 2001

A range of electron-rich organic molecules has been intercalated into MoS_2 by the method of exfoliation–reflocculation. Intercalation produces an expansion of the lattice in a direction perpendicular to the dichalcogenide layers, the magnitude of which suggests that in the majority of cases, the guest adopts an orientation in which the molecular plane is parallel to the dichalcogenide layers. This is further supported by the suppression of the majority of the vibrational modes in the inelastic neutron scattering spectrum. The introduction of polar substituents to naphthalene favours a perpendicular orientation of the guest in the interlayer space, permitting a higher degree of organic incorporation. The electron transport properties of MoS_2 are modified by intercalation and materials containing naphthalene and alkylated derivatives exhibit anomalous behaviour at low temperatures. EXAFS data provide evidence for a structural distortion, involving the formation of cation chains, in the naphthalene intercalate.

Introduction

In the continuing quest for materials with novel or enhanced properties, hybrid inorganic–organic systems have recently attracted much attention. Interaction at the microscopic level between inorganic and organic fragments frequently confers properties on the hybrids, which differ markedly from those of either component. Inorganic–organic nanocomposites have been prepared that exhibit remarkable mechanical, optical, electronic and magnetic properties which may be exploited in a range of applications including sensors,[1] molecular recognition,[2] magnetic films,[3] waveguides,[4] plastic superconductors[5] and lightweight structural composites.[6]

Intercalation carried out at ambient temperature[7,8] is generally topotactic and hence, in the case of layered hosts, the lamellar nature of the host persists into the product phase. Intercalation of layered materials therefore provides a means of producing materials in which organic and inorganic components are interleaved and in which the ratio of the two components may be varied in a continuous manner. The layered transition metal dichalcogenides are among the most studied host materials and a wide range of organic molecules has successfully been introduced by direct reaction: a comprehensive tabulation is given by Subba Rao and Shafer.[9] However, the accompanying redox process involving transfer of charge into vacant low-lying energy levels of the host imposes electronic constraints on the host material, resulting in lower reactivity of the layered dichalcogenides of group 6 transition metals compared to their group 4 and 5 analogues.[10]

The expansion of the interlayer space, which occurs when layered materials accommodate guest species, modifies the interlayer interactions which at large interlayer expansions may be weakened sufficiently for the layers to disperse completely. The resulting colloidal suspension of highly anisotropic particles is thermodynamically unstable with respect to reflocculation but may be stabilised by appropriate choice of solvent and/or pH. Lerf and Schöllhorn[11] demonstrated that solvated alkali metal dichalcogenides, $A_x(solv)[MS_2]$, exfoliate in solvents of high dielectric strength such as *N*-methyl formamide, when subjected to weak shear forces. Subsequently Nazar and Jacobson[12] showed that colloidal suspensions allow kinetic problems associated with the intercalation of bulky guest species to be overcome.

Single layer dispersions[13] therefore provide a means of synthesising previously inaccessible materials. In particular they afford an opportunity of extending the organic intercalation chemistry of the group 6 dichalcogenides. Joensen *et al.*[14] first reported that addition of water to the lithiated phase $LiMoS_2$ results in the evolution of hydrogen gas and the production of a colloidal suspension. Reflocculation of colloidal suspensions of MoS_2 in the presence of small organic molecules, including those which are poor electron donors, has been shown to lead to their incorporation in the van der Waals' gap.[15,16] Long chain organic polymers such as polyaniline (PANI),[17] polyethylene oxide[18] and polypyrrole[19] have also been introduced in this way, producing hybrid materials whose electronic properties differ markedly from those of the semiconducting MoS_2 parent material. For example, over the temperature range $50 \leqslant T/K \leqslant 300$, $(PANI)_{0.35}MoS_2$ appears to be metallic but its resistivity increases by three orders of magnitude at 8–9 K, suggesting a change to a semiconducting state. Recognising that many of the MoS_2 intercalates which exhibit unusual transport properties contain electron-rich polymeric guests, we have sought to prepare hybrid materials containing small electron-rich species.[20,21] Here we describe the synthesis and characterisation of a range of intercalates containing organic molecules with one or more aromatic rings.

Experimental

During a recent investigation of naphthalene intercalation,[20] the effect of a wide range of reaction variables was investigated. A high degree of reduction of Li_xMoS_2 is essential, as materials with lithium contents significantly less than one do not exfoliate completely, resulting in contamination of the organic intercalate with MoS_2. Production of well-ordered single phase naphthalene intercalates requires guest solutions to be close to saturation, since restacking of the layers results with more dilute solutions. No reflocculation occurs in the absence of acid, even on prolonged stirring of the single layer suspension and guest solution. Furthermore, no significant intercalation

†Presented at Solid State Chemistry 2000, Prague, Czech Republic, 4–8 September 2000.

 DOI: 10.1039/b007545k

was observed for stirring times of less than 7 days. The extent of intercalation of naphthalene increased with stirring time, attaining close to the geometrically limiting value after 14 days. Longer contact times did not lead to any increase in the degree of intercalation beyond this value.

Therefore the following procedure was adopted, which permits intercalation of small electron-rich organic molecules into the van der Waals' gap of MoS_2, with a high degree of reproducibility. MoS_2, previously prepared from the elements at high temperature, was treated with three equivalents of standardised 1.6 M n-butyllithium in distilled petroleum ether (bp 60–80 °C), under dry N_2. After stirring for 48 hours, the solid product was extracted by filtration, washed with petroleum ether and dried under vacuum. The product is a single-phase material with a hexagonal unit cell (typical lattice parameters: $a=3.312(45)$ Å, $c=6.394(18)$ Å) and a lithium content, as determined by flame emission spectroscopy, of 1.0 ± 0.02 per formula unit. Exfoliation was achieved by the addition to $LiMoS_2$ of sufficient deionised water to produce a suspension of typically 0.08 g ml^{-1} exfoliated MoS_2. The suspension was then sonicated for 30 minutes, prior to addition of the guest species in a suitable solvent (molar ratio of guest : $MoS_2=5:1$). The single layer dispersion[13] reflocculated on acidification to $pH\leqslant2$ with concentrated HCl and stirring was continued for a period of up to 3 weeks, after which the solid was separated, washed with water and solvent and vacuum dried. This procedure was also carried out omitting the guest species from the solvent at the reflocculation stage to produce a material hereafter denoted as reflocculated MoS_2.

Powder X-ray diffraction data were collected for all solid products using a Philips PA2000 powder diffractometer operating with nickel filtered Cu-Kα radiation. Sample compositions were determined by a combination of combustion analysis and thermogravimetry. The latter was performed using a DuPont Instruments 951 thermal analyser. Samples were heated in a flow of dry air over the temperature range 273–573 K at a heating rate of 5 K min^{-1}. Electron transport property measurements as a function of temperature were carried out on all intercalated phases using the 4-probe DC technique. Four 50 μm silver wires were attached to a cold-pressed ingot ($\sim6\times3\times1$ mm) by colloidal silver paint and connections made to a HP34401A multimeter. Samples were mounted in an Oxford Instruments CF1200 cryostat connected to an ITC502 temperature controller.

Naphthalene intercalates were further investigated by inelastic neutron scattering (INS) and extended X-ray absorption fine structure spectroscopy (EXAFS). INS data were collected for $(C_{10}H_8)_{0.15}MoS_2$, reflocculated MoS_2 and naphthalene using the TFXA spectrometer located at the ISIS spallation source. All samples were contained in aluminium foil sachets and data were collected for 15–20 h. Full details of the operation of the spectrometer have been given elsewhere.[22] Data manipulation was carried out using standard ISIS routines. After suitable normalisation, data for the reflocculated material were subtracted from those of the intercalated phase in an effort to remove the scattering from protons which were not associated with naphthalene molecules. Mo K-edge EXAFS data for $(C_{10}H_8)_{0.13}MoS_2$ were collected at room temperature in transmission mode on Station 9.2 at the SRS, Daresbury Laboratory. A Si(220) double crystal monochromator was used, detuned to reject 50% of the signal in order to minimise harmonics, and the monochromator angle calibrated using a 5 μm Mo foil. Detectors were ion chambers filled with a mixture of Ar and He. Samples, diluted with boron nitride, were placed on adhesive tape mounted in an aluminium holder. The programs EXCALIB, EXBACK and EXCURV98[23] were used to process the data. Four scans of 25 minutes were summed and a smooth background was removed from the raw data by fitting polynomials to both the pre- and post-edge regions. Calibration of phase shifts was performed using data collected on 2H-MoS_2. The data were Fourier filtered to exclude shells >4 Å where the statistics are poor.

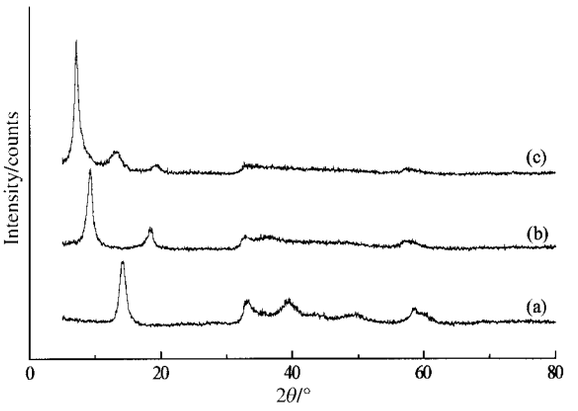

Fig. 1 Powder X-ray diffraction data for (a) poorly crystalline MoS_2 with an interlayer spacing of 6.2 Å, prepared by omitting the guest from the reflocculation step; (b) $(C_{10}H_8O_2)_{0.13}MoS_2$ showing the 001 and 002 reflections corresponding to an interlayer spacing of 9.7 Å; (c) $(C_{10}H_{12}N_2)_{0.35}MoS_2$ showing the 001, 002 and 003 reflections corresponding to an interlayer spacing of 12.4 Å.

Results

Exfoliation followed by reflocculation in the absence of a guest species produces a material whose powder X-ray diffraction data (Fig. 1(a)) are consistent with the formation of poorly crystalline restacked MoS_2. An interlayer spacing of 6.2 Å determined from the intense 001 reflection is similar to that in pristine 2H-MoS_2 [24] and indicates that there is no intercalation of solvent. In an effort to examine more closely the restacking of the layers, a sample of the colloidal dispersion was allowed to dry, at room temperature in air, on an X-ray diffraction slide and diffraction patterns (Fig. 2) recorded periodically. After a few hours' drying, an intense low angle peak at $2\theta=7°$ and a weaker feature at $2\theta=14°$ are evident. The appearance of a low angle reflection ($d=12.1$ Å) at short drying times has been attributed to the incorporation of a bilayer of water in the van der Waals' gap,[25,26] which is accompanied by the formation of a $2a_0\times a_0$ superstructure of 2H-MoS_2.[27] The intensity of the low angle reflection decreases markedly on drying for 5 days and disappears completely on prolonged drying when only the higher angle feature remains, indicative of the formation of

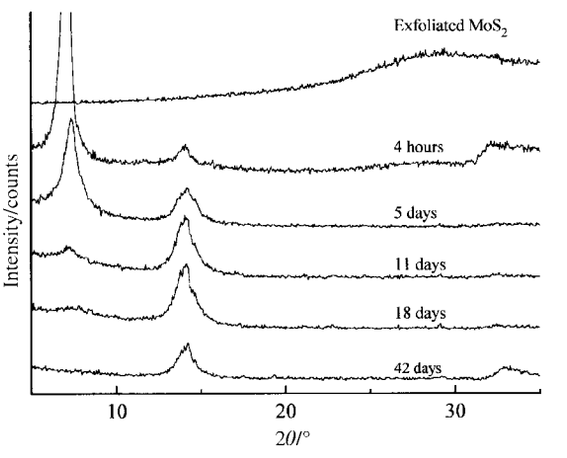

Fig. 2 Powder X-ray diffraction data recorded as a function of time for exfoliated MoS_2 allowed to dry at ambient temperature in air on an X-ray slide. The lowest angle peak corresponds to a *d*-spacing of 12.1 Å, consistent with a bilayer of water in the interlayer space.

Table 1 Compositions,[a] interlayer spacings and lattice expansions of organic intercalates of MoS_2

Reactant	Solvent	x in $(Guest)_xMoS_2$	Interlayer spacing/Å	Δc/Å
naphthalene	CH_2Cl_2	0.20	10.5	4.3
2-methylnaphthalene	CH_2Cl_2	0.19	10.5	4.3
2-ethylnaphthalene	CH_2Cl_2	0.09	9.7	3.5
1-chloromethylnaphthalene	CH_2Cl_2	0.36	13.8	7.6
1,5-dihydroxynaphthalene	CH_3CN	0.40	11.9	5.7
1,5-dihydroxynaphthalene	CH_3CN	0.13	9.7	3.5
1,5-diaminonaphthalene	CH_2Cl_2	0.22	9.9	3.7
1,5-diaminonaphthalene	CH_3CH_2OH	0.28	12.8/9.6	6.6/3.4
1,5-diaminonaphthalene dihydrochloride	H_2O	0.35	12.4	6.2
biphenyl	CH_2Cl_2	0.17	12.0	5.8
crystal violet	CH_2Cl_2	0.07	10.2	4.0
1,4-benzoquinone	CH_3CH_2OH	0.30	10.7	4.5
1,4-hydroquinone	CH_3CH_2OH	0.08	9.9	3.7
1,4-phenylenediamine	CH_3CH_2OH	0.11	9.2	3.0
1,4-phenylenediamine dihydrochloride	H_2O	0.12	9.5	3.3

[a]All compositions refer to the maximum degree of guest uptake, with the exception of 1,5-dihydroxynaphthalene for which a second product with a lower organic content, obtained at shorter reaction times, is reported.

poorly crystalline MoS_2. This is consistent with X-ray diffraction and Raman spectroscopic studies[28] which reveal that single layer suspensions, in which the molybdenum coordination is octahedral, revert to trigonal prismatic coordination on aging.

A variety of mono- and 1,5-disubstituted naphthalene derivatives and related electron-rich molecules (Table 1) have been intercalated into MoS_2. Powder X-ray diffraction data of the products (for which representative data are presented in Fig. 1) are similar to those of the restacked material. However, the 00*l* reflections are shifted to lower angles, which signifies an increase in the interlayer spacing, resulting from incorporation of the guest molecules in the van der Waals' gap of MoS_2. The observed lattice expansions, Δc, are presented in Table 1, together with sample compositions. The magnitude of Δc provides an indirect indicator of the orientation of the guest molecule. The effective ring thickness of aromatic molecules has been estimated as 3.7 Å.[29] Therefore a comparable interlayer expansion may be taken to indicate a guest molecule adopting an orientation in which the molecular plane is parallel to the MoS_2 layers. The in-plane dimensions of a naphthalene molecule have been determined by molecular modelling[30] to be *ca.* 6.8×5.1 Å. This would result in a geometrically limiting composition for a monolayer of molecules in this orientation of *ca.* 0.25 guest molecules per MoS_2, although this value will be reduced by the presence of one or more substituents. For a single ring system, similar considerations lead to a somewhat higher upper limit of *ca.* 0.4 guest molecules per mole of MoS_2. Examination of Table 1 suggests that naphthalene and its alkylated derivatives are incorporated with the molecular plane parallel to the disulfide layers. However a significantly greater uptake of guest and a larger Δc are observed for the chloromethyl and dihydroxy derivatives. This, together with consideration of the dimensions of these molecules, suggests that the presence of polar substituents favours an orientation in which the guest molecule is aligned perpendicular to the MoS_2 layers, although a parallel orientation appears to be favoured at the low degrees of incorporation of 1,5-dihydroxynaphthalene obtained at shorter reaction times. Intercalation of 1,5-diaminonaphthalene shows a greater dependence on reaction conditions. On acidification, precipitation of the guest as the dihydrochloride salt was observed from solution in dichloromethane. However, this salt is appreciably soluble in water and could therefore be removed by washing, yielding a product in which the molecule appears to adopt a parallel orientation. Use of a saturated aqueous solution of the dihydrochloride salt in place of the organic solution produced a material with a higher degree of organic incorporation and an interlayer expansion comparable with the dihydroxy derivative. Interestingly, when the neutral guest was introduced as a solution in ethanol, reflections corresponding to both interlayer expansions could be observed (6.6 and 3.4 Å). In biphenyl, intramolecular rotation about the C–C bond would allow the rings to adopt a non-coplanar orientation, increasing the effective size of the molecule and accounting for the large Δc observed even at relatively low degrees of incorporation.. The smaller Δc observed for crystal violet is comparable with the ring thickness. This suggests an orientation in which the aromatic rings lie parallel to the MoS_2 layers. The organic incorporation is close to the geometric limit (0.11) for this orientation. The extent of intercalation of the single ring molecules is generally low and all appear to adopt a parallel orientation.

MoS_2 is a semiconductor with an activation energy of 0.235 eV below 790 K.[31] Transport property data for the intercalated phases are summarised in Table 2. As measurements were performed on pressed pellets, conduction will be particularly sensitive to defects and some caution must be exercised in comparing resistivity values obtained for different materials. All materials show thermally activated conduction (Fig. 3(a)), indicating that semiconducting behaviour persists on exfoliation and reflocculation. While attempts to fit a simple Arrhenius expression to these data were unsuccessful, plots of $\ln(\rho)$ *vs.* $T^{-1/4}$ are generally linear (Fig. 3(b)) over extended ranges of temperature, which are shown in Table 2. The naphthalene and alkylated naphthalene intercalates exhibit low-temperature anomalies in $\rho(T)$ (Fig. 3(c)). The resistivity of $(C_{10}H_8)_{0.13}MoS_2$ increases on cooling to 100 K at which

Table 2 Summary of transport property data for organic intercalates of MoS_2

Material	ρ_{300K}/Ω cm	ρ_{80K}/Ω cm	Range in K over which $\ln(\rho)$ *vs.* $T^{-1/4}$ is linear
$(C_{10}H_8)_{0.11}MoS_2$	5	3.6×10^3	100–220
$(C_{11}H_{10})_{0.19}MoS_2$	4	1.3×10^4	80–300
$(C_{12}H_{12})_{0.09}MoS_2$	5	2.8×10^4	80–200
$(C_{11}H_9Cl)_{0.36}MoS_2$	6.6×10^2	2.2×10^5	140–300
$(C_{10}H_8O_2)_{0.40}MoS_2$	5	6.7×10^2	100–300
$(C_{10}H_8O_2)_{0.13}MoS_2$	1.3×10^1	8.9×10^2	80–300
$(C_{10}H_{12}N_2)_{0.22}MoS_2$	5.5×10^1	1.3×10^4	85–300
$(C_{10}H_{12}N_2)_{0.35}MoS_2$	2.5×10^1	3.6×10^4	80–300
$(C_{12}H_{10})_{0.17}MoS_2$	4	1.8×10^3	80–300
$(C_{25}H_{30}N_3)_{0.07}MoS_2$	1.0×10^3	5×10^4	non-linear
$(C_6H_4O_2)_{0.30}MoS_2$	4	5.3×10^2	100–300
$(C_6H_6O_2)_{0.08}MoS_2$	2.4×10^2	1.02×10^6	125–250
$(C_6H_8N_2)_{0.11}MoS_2$	1	3.7×10^1	100–300

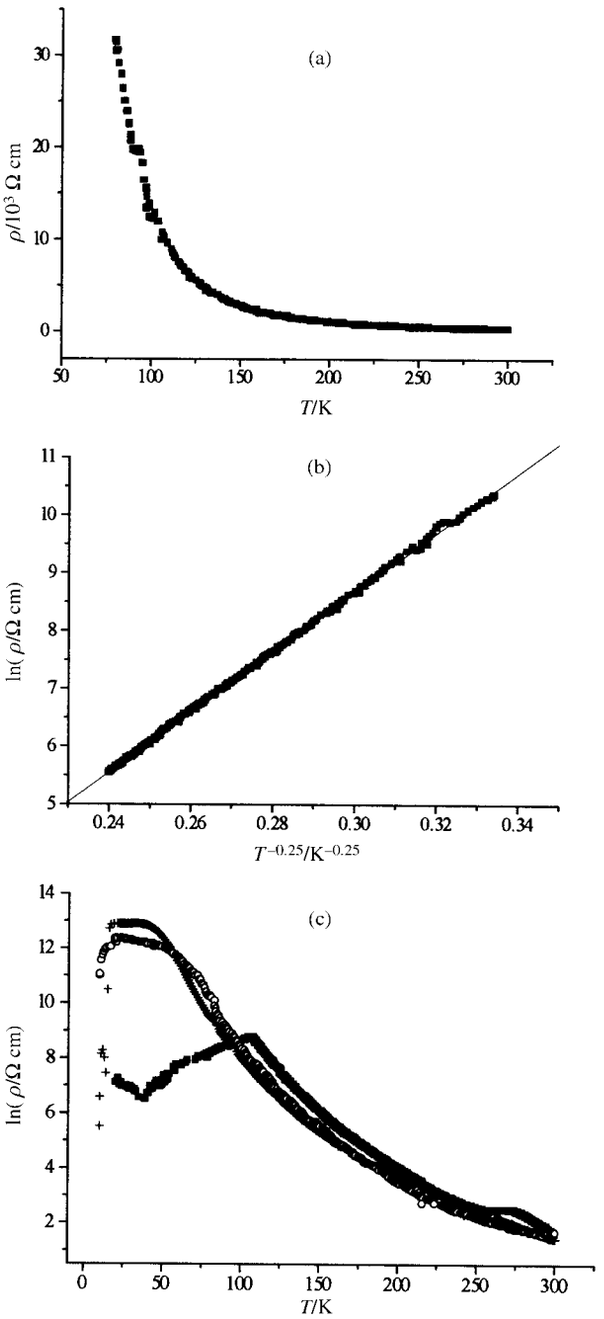

Fig. 3 (a) Representative electrical transport property data for the semiconducting phases. The data shown are those of $(C_{10}H_{12}N_2)_{0.35}MoS_2$. (b) $T^{-1/4}$ dependence of ln(ρ), the solid line showing the best linear fit. (c) Electrical transport data for $(C_{10}H_8)_{0.11}MoS_2$ (solid points), $(C_{11}H_{10})_{0.19}MoS_2$ (crosses) and $(C_{12}H_{12})_{0.09}MoS_2$ (open points).

temperature d(lnρ)/dT changes sign, and the resistivity passes through a shallow minimum before increasing slightly on cooling further. Intercalates containing the alkylated derivatives show similar anomalies at temperatures of 33 and 23 K for methyl and ethyl substituents respectively.

Comparison of the INS spectrum of $(C_{10}H_8)_{0.15}MoS_2$ with that of naphthalene (Fig. 4) reveals significant changes to the low-energy density of states region as a result of guest–host interaction. Furthermore the *relative* intensities of the majority of the vibrational modes are significantly reduced on intercalation. Only three modes may be clearly identified in the INS spectrum. The features at 460, 960 and 1154 cm^{-1} may be assigned, on the basis of *ab initio* force field calculations,[32] as

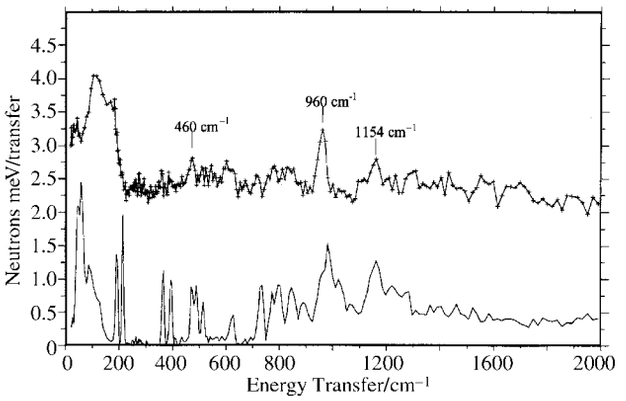

Fig. 4 Inelastic neutron scattering spectra of naphthalene (lower trace) and $(C_{10}H_8)_{0.15}MoS_2$ (upper trace). Features referred to in the text are indicated.

a C–C–C torsional mode (calculated 471 cm^{-1}), an out-of-plane CH bend (calculated 981 cm^{-1}) and in-plane CH bend (calculated 1156 cm^{-1}) respectively.

The k^3-weighted EXAFS data together with the Fourier transformed data for crystalline 2H-MoS_2 used for calibration purposes are shown in Fig. 5(a), and the corresponding data for $(C_{10}H_8)_{0.13}MoS_2$ in Fig. 5(b). Features at 2.407(4) and 3.166(3) Å in the data for 2H-MoS_2 are in excellent agreement with the Mo–S and Mo–Mo distances expected from the crystallographic structure. In the data for the intercalate, a strong feature corresponding to the sulfur shell is again apparent at a distance of *ca.* 2.4 Å. However, three features are observed at longer distances, arising from next-nearest neighbour molybdenum atoms. Consequently the data could not be fitted using the 2H-MoS_2 structural model, in which six equidistant neighbours surround each molybdenum. Therefore a model in which there are three different Mo–Mo distances was fitted to the data. Least squares refinement of distances and Debye–Waller factors produced a good quality of fit (discrepancy index, $R=22\%$). Attempts to refine coordination numbers simultaneously produced only a marginal improvement in the fit and a reduction in the sum of molybdenum neighbours, to physically unrealistic values significantly below six. Refinement of coordination numbers and distances, whilst holding the Debye–Waller factors at their previously refined values, produced little change in coordination numbers from their nominal values. This suggests that the coordination numbers and Debye–Waller factors are strongly correlated. Consequently, all coordination numbers were fixed at their ideal values in the final cycles of refinement, which produced the structural model summarised in Table 3.

Table 3 Refined parameters[a] derived from analysis of Mo K-edge EXAFS data for a crystalline 2H-MoS_2 standard and the intercalate $(C_{10}H_8)_{0.13}MoS_2$

Sample	Shell	Occupation number[b]	Distance/Å	Debye–Waller factor/Å^2
2H-MoS_2 ($R=15\%$)	S	6	2.407(4)	0.0086(5)
	Mo	6	3.166(3)	0.0059(2)
	S	6	3.971(20)	0.014(4)
$(C_{10}H_8)_{0.13}MoS_2$ ($R=22\%$)	S	6	2.422(4)	0.0150(6)
	Mo	2	2.748(6)	0.016(1)
	Mo	2	3.160(10)	0.018(2)
	Mo	2	3.769(27)	0.024(6)

[a]The uncertainties quoted are those derived from least-squares fitting procedures. [b]Constrained at crystallographic values.

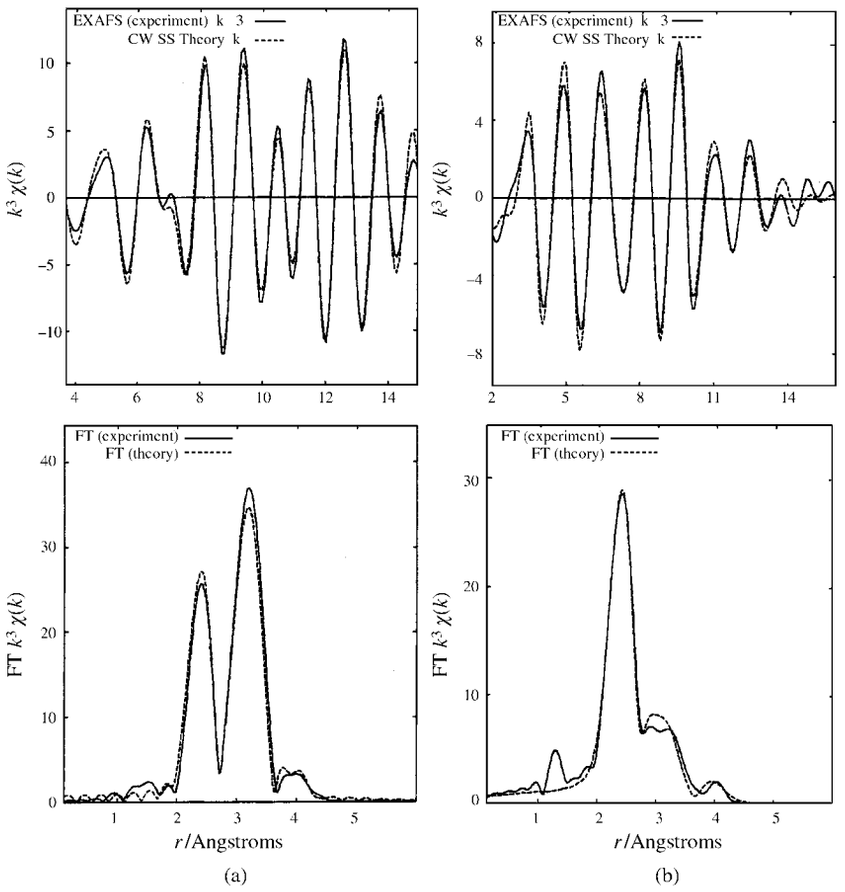

Fig. 5 The k^3-weighted Fourier filtered Mo K-edge EXAFS spectrum (upper plots) together with its Fourier transform (lower plots) for (a) the 2H-MoS_2 standard and (b) $(C_{10}H_8)_{0.13}MoS_2$. The solid line shows experimental data and the dashed line shows the theoretical data.

Discussion

Exfoliation–reflocculation has allowed a wide range of molecules with extended π-electron networks to be intercalated into MoS_2. Intercalation expands the interlayer spacing by an amount which generally correlates well with the molecular dimensions of the guest. Lattice expansions of $\leqslant 4.5$ Å appear to correspond to planar guest molecules being oriented with the molecular plane parallel to the dichalcogenide layers. Support for this is provided by observed degrees of organic incorporation which are below the geometrically limiting values for this arrangement. Furthermore, INS data for the naphthalene intercalate reveal that the majority of the vibrational modes of the guest are suppressed, consistent with the molecule residing in a highly restricted site in the intercalate.

All materials exhibit a $T^{-1/4}$ dependence of $\ln\rho$ over an extended range of temperature. This is characteristic of a variable-range-hopping conduction mechanism,[33] suggesting that conduction is dominated by hopping of charge carriers between states localised on opposite sides of the Fermi energy. Localisation of states at the band edge may be a manifestation of the effects of disorder, a measure of which is provided by relatively high Debye–Waller factors for the molybdenum shells, determined in the EXAFS study. EXAFS data also provide evidence for a structural distortion in the naphthalene intercalate. Although the local coordination of molybdenum is little altered from that in 2H-MoS_2 (Mo–S = 2.422(4) Å), there are significant changes to the molybdenum sublattice. In the crystalline phase, each molybdenum is coordinated by six equidistant neighbours (Mo–Mo = 3.166(3) Å) in a hexagonal array. However, three different Mo–Mo distances are observed in the intercalate. A molybdenum atom has two neighbours at a distance of 3.160(10) Å, which is little altered from that of the pristine material, and two pairs of neighbours at longer and shorter distances. This is consistent with a structural model in which an intralayer distortion produces zigzag chains of molybdenum atoms (Fig. 6), giving rise to a $2a_0 \times a_0$ (or equivalently $\sqrt{3}a_0 \times a_0$) superstructure of 2H-MoS_2. Heising and Kanatzidis[34] have recently identified such a superstructure in restacked MoS_2. Their electron diffraction data revealed the presence of infinite zigzag chains of molybdenum in which the shortest Mo–Mo distance is *ca.* 2.92 Å. Moreover their data suggest that earlier observations of a $2a_0 \times 2a_0$ superstructure arose from rotational disorder between successive MoS_2 layers. Distortion of layered MX_2 structures containing d^2 ions to form zigzag chains has been predicted by Rovira and Whangbo.[35] A similar distortion of VS_2 layers has been observed[36] in ternary sulfides and is associated with the onset of

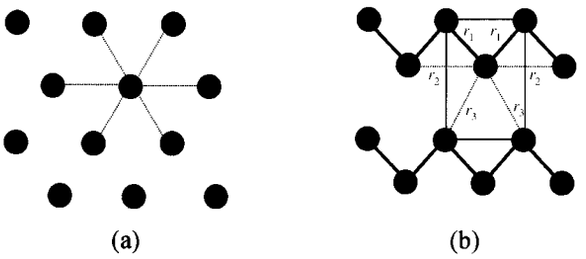

Fig. 6 (a) Layer of cations in MoS_2 where each cation has six molybdenum neighbours at a distance of 3.166(3) Å. (b) Proposed intralayer distortion involving the formation of zigzag chains of cations in $(C_{10}H_8)_{0.13}MoS_2$ in which $r_1 = 2.748(6)$ Å, $r_2 = 3.160(10)$ Å and $r_3 = 3.769(27)$ Å. The thin solid line shows a $\sqrt{3}a_0 \times a_0$ unit cell consistent with the results[34] of an electron crystallography study on restacked MoS_2.

metallisation in the non-stoichiometric series $NiCr_{2-x}V_xS_4$ at $x \approx 0.6$.[37] The calculations of Canadell *et al.*[38] for octahedral MS_2 layers demonstrate that such a distortion gives rise to a pronounced dispersion of one component of the t_{2g} manifold. The semiconducting behaviour of the materials prepared here indicates trigonal prismatic coordination of molybdenum in the intercalated phases, with the result that the lowest-lying orbital will be a filled $d(z^2)$ orbital. The relatively short intrachain cation–cation separation would favour formation of a one-dimensional band involving higher-lying orbitals. Furthermore, the observed weak paramagnetism[21] of these materials provides evidence for a degree of charge transfer between guest and host. This, together with the one-dimensional character introduced by the distortion, may be responsible for the anomalous low-temperature transport properties of the naphthalene intercalate and related phases. The low temperature resistivity is considerably higher than that expected for a metal, which suggests that the change in sign of $d(\ln(\rho))/dT$ is more likely to be associated with charge density wave formation, a characteristic feature of low-dimensional systems,[39] than with a semiconductor to metal transition. Further investigation of the structural properties of these poorly crystalline phases is underway in an effort to rationalise their observed transport behaviour.

Acknowledgements

We thank Heriot-Watt University and the EPSRC for studentships for L. K. and A. M. respectively and the EPSRC for a grant in support of our neutron scattering programme. The assistance of Drs R. Strange, SRS, Daresbury Laboratory and W. Kagunya, ISIS, Rutherford Appleton Laboratory, with the collection of EXAFS and INS data respectively, is gratefully acknowledged. Access to the SRS was provided under the auspices of the DARTS scheme through funding by the EPSRC. We wish to thank Dr S. J. Hibble, University of Reading for useful discussions concerning EXAFS data.

References

1 E. R. Kleinfeld and G. S. Ferguson, *Chem. Mater.*, 1995, **7**, 2327.
2 G. Cao, M. A. Garcia, M. Alcalá, L. F. Burgess and T. E. Mallouk, *J. Am. Chem. Soc.*, 1999, **114**, 7574.
3 M. Clemente-León, C. Mingotaud, B. Agricole, C. J. Gómez-Garcia, E. Coronado and P. Delhaès, *Angew. Chem., Int. Ed. Engl.*, 1997, **36**, 1114.
4 C. Xu, L. Eldada, C. Wu, R. A. Norwood, L. W. Shacklette, J. T. Yardley and Y. Wei, *Chem. Mater.*, 1996, **8**, 2701.
5 H.-L. Tsai, J. L. Schindler, C. R. Kannewurf and M. G. Kanatzidis, *Chem. Mater.*, 1997, **9**, 875.
6 T. Lia and T. Pinnavaia, *Chem. Mater.*, 1994, **6**, 2216.
7 A. M. Chippindale, P. G. Dickens and A. V. Powell, *Progr. Solid State Chem.*, 1991, **21**, 133.
8 A. V. Powell, *Annu. Rep. Prog. Chem. Sect. C*, 1993, **90**, 177.
9 G. V. Subba Rao and M. W. Shafer, in *Intercalated Layered Materials*, ed. F. Lévy and D. Reidel, Dordrecht, 1979, p. 99.
10 R. H. Friend and A. D. Yoffe, *Adv. Phys.*, 1987, **36**, 1.
11 A. Lerf and R. Schöllhorn, *Inorg. Chem.*, 1977, **16**, 2951.
12 L. F. Nazar and A. J. Jacobson, *J. Chem. Soc., Chem. Commun.*, 1986, 570.
13 A. J. Jacobson, in *Comprehensive Supramolecular Chemistry*, ed. J. L. Atwood, J. E. D. Davies, D. D. MacNicol and F. Vögtle, Pergamon, Oxford, 1996, vol. 7, ch. 10.
14 P. Joensen, R. F. Frindt and S. R. Morrison, *Mater. Res. Bull.*, 1986, **21**, 457.
15 H. Tagaya, T. Hashimoto, M. Karasu, T. Izumi and K. Chiba, *Chem. Lett.*, 1991, **12**, 2113.
16 W. M. R. Divigalpitiya, R. F. Frindt and S. R. Morrison, *Science*, 1989, **246**, 369.
17 M. G. Kanatzidis, R. Bissessur, D. C. DeGroot, J. L. Schindler and C. R. Kannewurf, *Chem. Mater.*, 1993, **5**, 595.
18 R. Bissessur, M. G. Kanatzidis, J. L. Schindler and C. R. Kannewurf, *J. Chem. Soc., Chem. Commun.*, 1993, 1582.
19 L. Wang, J. Schindler, J. A. Thomas, C. R. Kannewurf and M. G. Kanatzidis, *Chem. Mater.*, 1995, **7**, 1753.
20 L. Kosidowski and A. V. Powell, *Chem. Commun.*, 1998, 2201.
21 A. V. Powell, L. Kosidowski and A. McDowall, *Mol. Cryst. Liq. Cryst.*, 2000, **341**, 125.
22 J. Penfold and J. Tomkinson, Rutherford Appleton Laboratory Report RAL-86-019, 1986.
23 N. Binsted, EXCURV98, CCLRC Daresbury Laboratory Computer Program, 1998.
24 JCPDS PDF Card No. 37-1492, Joint Committee on Powder Diffraction Standards, Swarthmore, PA.
25 P. Joensen, E. D. Crozier, N. Alberding and R. F. Frindt, *J. Phys. C: Solid State Phys.*, 1987, **20**, 4043.
26 D. Yang, S. Jimenez Sandoval, W. M. R. Divigalpitiya, J. C. Irwin and R. F. Frindt, *Phys. Rev. B*, 1991, **43**, 12053.
27 X. R. Qin, D. Yang, R. F. Frindt and J. C. Irwin, *Phys. Rev. B*, 1991, **44**, 3490.
28 S. Jimenez Sandoval, D. Yang, R. F. Frindt and J. C. Irwin, *Phys. Rev. B*, 1991, **44**, 3955.
29 E. Mack, *J. Phys. Chem.*, 1937, **41**, 221.
30 Molecular modelling was performed with the CAChe program, version 4.1, Oxford Molecular, 1999.
31 S. H. El-Mahalawy and B. L. Evans, *Phys. Status Solidi B*, 1977, **79**, 713.
32 H. Sellers, P. Pulay and J. E. Boggs, *J. Am. Chem. Soc.*, 1985, **107**, 6487.
33 N. F. Mott, *J. Non-Cryst. Solids*, 1968, **1**, 1.
34 J. Heising and M. Kanatzidis, *J. Am. Chem. Soc.*, 1999, **121**, 638.
35 C. Rovira and M-H. Whangbo, *Inorg. Chem.*, 1993, **32**, 4094.
36 A. V. Powell, D. C. Colgan and P. Vaqueiro, *J. Mater. Chem.*, 1999, **9**, 485.
37 P. Vaqueiro, M. Bold, A. V. Powell and C. Ritter, *Chem. Mater.*, 2000, **12**, 1034.
38 E. Canadell, A. LeBeuze, M. Abdelaziz El Khalifa, R. Chevrel and M. H. Whangbo, *J. Am. Chem. Soc*, 1989, **111**, 3778.
39 G. Grüner, in *Physics and Chemistry of Low-Dimensional Inorganic Conductors*, ed. C. Schlenker, J. Dumas, M. Greenblatt and S. van Smaalen, *NATO ASI Ser. B*, 1996, vol. 354, p. 101.